Ocean Sci. J. (2018) 53(3):583–594
http://dx.doi.org/10.1007/s12601-018-0020-4

Available online at http://link.springer.com

SpringerLink

Article

Ocean Science Journal

pISSN 1738-5261
eISSN 2005-7172

# Wave-induced Maintenance of Suspended Sediment Concentration during Slack in a Tidal Channel on a Sheltered Macro-tidal Flat, Gangwha Island, Korea

**Guan-hong Lee[1] and KiRyong Kang[2]***

[1]*Department of Oceanography, College of Natural Sciences, Inha University, Incheon 22212, Korea*
[2]*National Institute of Meteorological Sciences, Korea Meteorological Administration, Seogwipo 63568, Korea*

Received 11 May 2017; Revised 1 February 2018; Accepted 27 May 2018


**Abstract** – A field campaign was conducted to better understand the influence of wave action, in terms of turbulence and bed shear stress, on sediment resuspension and transport processes on a protected tidal flat. An H-frame was deployed in a tidal channel south of Gangwha Island for 6 tidal cycles during November 2006 with instrumentation including an Acoustic Doppler Velocimeter, an Acoustic Backscatter System, and an Optical Backscatter Sensor. During calm conditions, the current-induced shear was dominant and responsible for suspending sediments during the accelerating phases of flood and ebb. During the high-tide slack, both bed shear stress and suspended sediment concentration were reduced. The sediment flux was directed landward due to the scour-lag effect over a tidal cycle. On the other hand, when waves were stronger, the wave-induced turbulence appeared to keep sediments in suspension even during the high-tide slack, while the current-induced shear remained dominant during the accelerating phases of flood and ebb. The sediment flux under strong waves was directed offshore due to the sustained high suspended sediment concentration during the high-tide slack. Although strong waves can induce offshore sediment flux, infrequent events with strong waves are unlikely to alter the long-term accretion of the protected southern Gangwha tidal flats.

**Keywords** – wave action, turbulence, bed shear stress, tidal flat, suspended sediment, scour-lag effect

## 1. Introduction

Tidal flats are important ecosystems, supporting large wildlife populations such as shellfish, fish and birds. The maintenance of a healthy ecosystem is closely linked to the stability of the tidal flats, which are under stress due to climate change and extensive coastal development. From the sedimentological point of view, the stability of tidal flats is maintained by the delicate balance between deposition and erosion. Thus, the understanding of sedimentary processes in the tidal flats is immensely important from both ecological and sedimentological viewpoints.

Tidal flats are characterized by a regular rise and fall in water levels. In such environments, tides are considered as the primary controlling factor for hydrodynamics and sediment transport. Suspension processes of sediment transport occur during periods of flow acceleration, while deposition of suspended sediment occurs during periods of negligible velocity or slack water periods. In the absence of waves, the net sediment flux is generally onshore due to settling and scour lag effects (e.g., Christie et al. 1999; Green and Coco 2014; Le Hir et al. 2000; Talke and Stacey 2008).

Although secondary, waves are regarded as exerting an important influence on tidal flat dynamics in that bed stress caused by waves can be dominant or comparable to the current-induced stress (Hu et al. 2017; Janssen-Stelder 2000; Le Hir et al. 2000; Green and Coco 2007, 2014; Verney et al. 2007). Moreover, nonlinear interaction of waves and currents increases bed shear stresses, promoting erosion on the tidal flats (Anderson and Pejrup 2001; Brand et al. 2010; Christie et al. 1999; Talke and Stacey 2008; Zhu et al. 2016). As described above, overall processes of sediment transport under the presence or absence of waves are well documented for intertidal flats. However, the effects of waves during the high-tide slack water are less well documented. In particular,

*Corresponding author. E-mail: krkang@korea.kr

the dynamic aspect of wave-induced turbulence and its effect on sediment suspension as well as the net sediment flux over a tidal cycle remain poorly known. During a strong storm event in November 2006, a unique opportunity was given to observe flow and suspended sediment concentration (SSC) under strong waves on the intertidal channel of the sheltered Gangwha tidal flat, Korea. In this paper, we investigated how waves and currents affected turbulence and sediment suspension over a tidal cycle. We examined the conditions necessary for waves to maintain sediments in suspension during the high-tide slack. The consequential effects of waves on morphology were evaluated in terms of sediment flux, which provided an insight into the general evolution of the Gangwha tidal flats.

## 2. Field Experiment and Data Analysis

**Study site and experimental design**

Tidal flats are extensively developed around Gangwha Island at the mouth of the Han River, Korea (Fig. 1A). The total area of the tidal flat is approximately 105 $km^2$ at the low tide and about 85% (90 $km^2$) of the area is found along the southern shores of Gangwha Island (Woo and Je 2002). The tidal flat extends up to 6 km from the shoreline during the low tides.

Tides are semidiurnal with a mean tidal range of 6.5 m. Spring tidal range reaches up to 10 m. Winds are monsoonal with strong northwesterly winds during the winter season and gentle southerly winds during the summer. Waves are relatively stronger during the winter, but wave height rarely exceeds 1 m on the tidal flats because of wave-energy dissipation over extensive sand shoals in the inner Gyeonggi Bay.

Sediments on the tidal flat are mainly derived from the Han River during high freshwater discharges over the summer season from June to August. Sedimentary facies become muddier from east to west across the southern Gangwha tidal flat (Woo and Je 2002; Choi and Dalrymple 2004). This transition of sedimentary facies is related to the density of the channel network: mud facies to high density and sand facies to low density of channel networks (Choi et al. 2011).

The tidal flat off the southeast corner of Gangwha Island (hereafter East Donggum tidal flat) consists of mud facies with densely distributed tidal channels (Fig. 1A) (Choi et al. 2011). The approximately 2.5 km wide flat is dissected by three main tidal channels, and these main channels divide further into a series of dendritic drainage systems. The major tributary channels are usually 1–2 m deep and 4–5 m wide at the bankful stage. The system is typical of channels along the East Donggum tidal flat. Surficial sediments are predominantly mud with a mean grain size of 6–7 φ and the sedimentation rate in the south of Donggum Island estimated at about 2–4 cm/yr (Woo and Je 2002).

A field experiment was conducted in a secondary channel of the East Donggum tidal flat from November 6–8, 2006 (Fig. 1A). An instrument package was deployed on an H-frame in the center of the wide (~20 m at the flat level) and deep (> 2 m) secondary tidal channel that runs north to south (37°36'33.91"N, 126°31'58.8"E) (Fig. 1B). The instruments on the H-frame included an Acoustic Doppler Velocimeter (ADV), an Acoustic Backscatter Sensor (ABS) and an Optical Backscatter Sensor (OBS) (Fig. 1B). The 5-MHz ADV system (Sontek ADV Ocean-Hydra) measured flow velocity at 10 Hz for burst durations of about 7 minutes at 10 minute intervals at the nominal elevation of 27 cm above the bed (ab). The ADV system also measured the water depth with built-in pressure sensor at the same sampling scheme for the velocity. The three-transducer ABS was placed at about 1 m ab, looking downward and measuring suspended sediment concentration (SSC) profiles at 1-cm intervals. The Seapoint OBS collected SSC at the same height for the flow measurement of the ADV. The ABS and OBS had the same sampling scheme as the ADV. Unfortunately, the ABS malfunctioned throughout the experiment and the OBS stopped collecting data on November 6, 2006 and thus their data are not used in this paper except for the OBS data used for the calibration of ADV signal strength into SSC.

**Flow data analysis and bed shear stress**

The burst-averaged water depth from the ADV was obtained by averaging $h(t)$, which is the burst time series of hydrostatic depth computed from the pressure series $p(t)$ as

$$h(t) = [(p(t)-p_a(t))/\rho g] + z_p \quad (1)$$

where $p_a$ is the atmospheric pressure obtained by the Korea Meteorological Administration (KMA), ρ is the water density, $g$ is the gravitational acceleration, and $z_p$ is the elevation of the pressure sensor. The energy-based significant wave height, $H_{mo}$, was calculated by the following definition,

$$H_{mo} = 4\sqrt{m_o} \quad (2)$$

where $m_o$ is the variance of sea surface elevation (Tucker

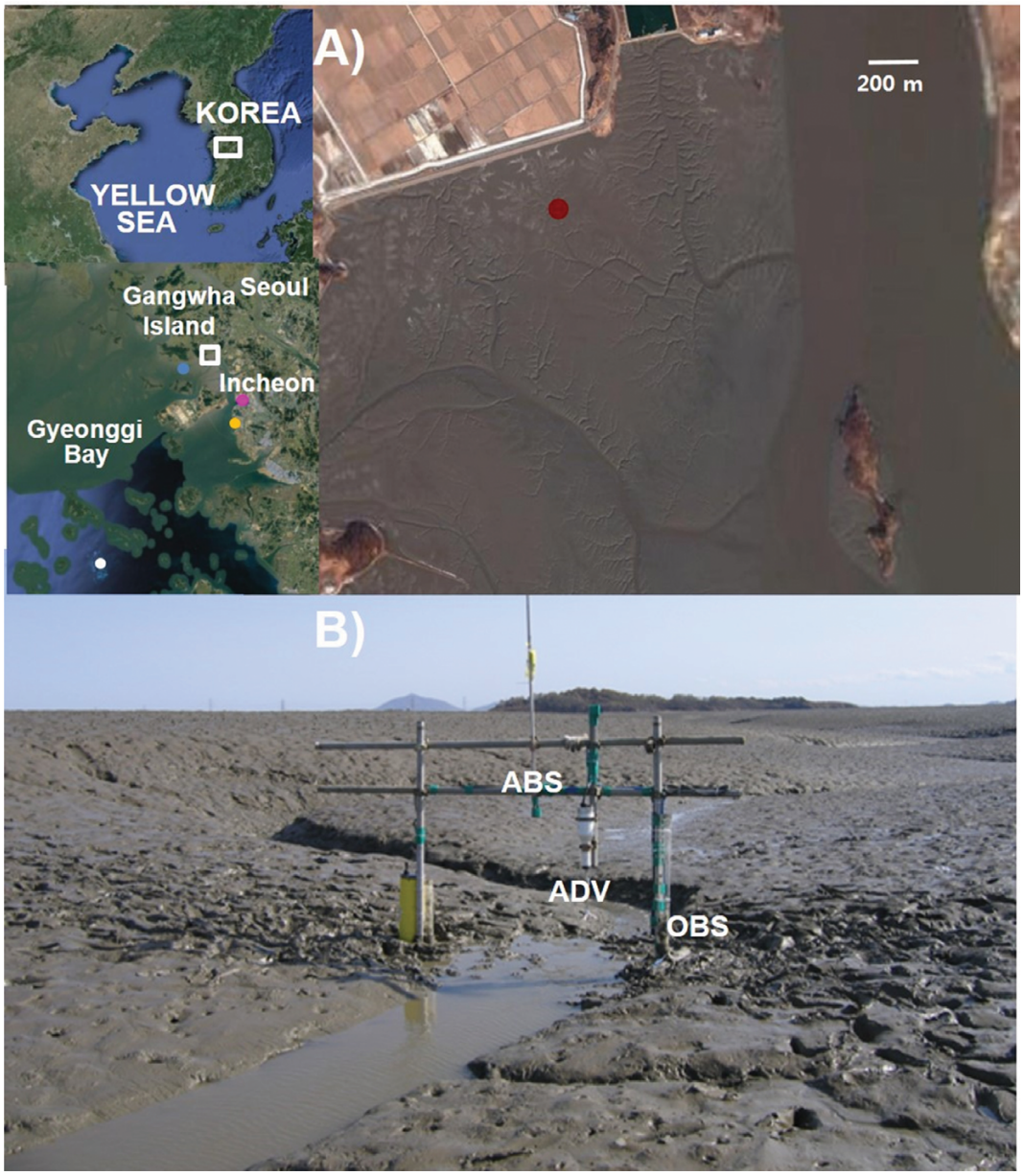


**Fig. 1.** A) Study site of East Donggum tidal flat. B) Configuration of Inha H-frame with Acoustic Backscatter Sensor, Acoustic Doppler Velocimeter and Optical Backscatter Sensor in a tidal channel. The red dot indicates the location of the field experiment in the secondary tidal channel. The white, pink, yellow and blue dots represent the Korean Meteorological Administration (KMA)'s Deokjeok wave buoy, KMA's Incheon wave and meteorological station, the Korea Hydrographic and Oceanographic Agency (KHOA)'s Incheon tidal station and the Korea Institute of Ocean Science and Technology (KIOST)'s wave buoy, respectively

and Pitt 2001). The wave period $T_p$ was determined from the peak frequency, $\omega$. Based on linear wave theory, the wave orbital velocity $u_b$ was calculated by the following equation,

$$u_b = \frac{\omega a}{\sinh(kh)} \tag{3}$$

where $k$ is the wave number and $a$ is the wave amplitude.

In this study, the ADV flow measurement captured variability from mean currents, wave motions, and turbulence. In the presence of waves, bed shear stress is estimated by the separation of the wave-induced and turbulence-induced variances of each fluctuating velocity component. In this paper, we used the inertial dissipation method of the w-component ($u_{*c\_idm}$) as the effect of vertical wave-induced velocity is small (Soulsby and Humphery 1990). This method has been successfully applied to different environments

such as estuaries (Kim et al. 2000), inner shelf environments (Lee et al. 2003), and tidal flats (Zhu et al. 2016). As important as the separation of wave-induced shears from turbulence is, it is also instructive to assess the combined effect of waves and currents ($u_{*c\_tke}$). The absolute intensity of velocity fluctuations, E, was obtained as,

$$E = \frac{\overline{u'^2} + \overline{v'^2} + \overline{w'^2}}{2}, \quad (4)$$

where u, v and w are x, y, z-velocity, respectively. The prime indicates velocity fluctuations, while the overbar represents the temporal mean. From Eq. 4, it is noted that both wave and turbulence variances are considered. Near the bed where energy production is equal to energy dissipation, the bed shear stress is proportional to the turbulent kinetic energy such that $t_{tke} = C_{tke}E$ (Soulsby and Dyer 1981; Kim et al. 2000). Various $C_{tke}$ values are proposed in the literature within the range of 0.18–0.21 (e.g. Soulsby 1983; Soulsby and Dyer 1981; Talke and Stacey 2008), but the constant value of 0.19 has been widely used (e.g. Kim et al. 2000; Lee et al. 2003; Shi et al. 2016; Verney et al. 2007).

Another method for estimating the shear velocity is to use a wave-current interaction model. Wave-current interaction models are usually employed to predict shear velocity due to currents ($u_{*c\_gm}$) and shear velocity due to the combined effect of waves and currents ($u_{*cw\_gm}$) from knowledge of currents (burst-averaged current velocity, $u_c$) at a point, near-bottom orbital velocity ($u_b$), and physical bottom roughness characteristics. The bed roughness was defined as the sum of the grain roughness and the movable roughness, where the grain roughness is on the order of the grain diameter ($2.5d_s$, where $d_s$ = 20 mm is the mean grain size) and the movable roughness was calculated following Xu and Wright (1995). The Grant and Madsen wave-current interaction model (Grant and Madsen 1986; hereinafter referred to as GM) was applied because of its simplicity and wide usage in the literature. The GM model and its application are described in more detail and has been successfully applied to inner shelf conditions (e.g., Lee et al. 2002) and in a moderate sense to tidal flats (e.g., Carlin et al. 2016; MacVean and Lacy 2014).

Standard transformation of time-series observations of flow velocities was used to obtain Fourier spectra (e.g., Bendat and Piersol 2010). Following conventional pre-whitening of time series, 4096 data were partitioned into segments of equal length of 256 data and with 50 percent overlap with adjoining segments. A Hanning window was applied to each segment before Fourier transformation. The resulting spectra were arithmetically averaged with the 95 percent confidence intervals corresponding to 0.64–1.79 times the smoothed spectral estimates of velocity data.

**Suspended sediment concentration calibration**

Sediment samples were taken at the beginning of the field experiment for laboratory calibration of the OBS and particle size analysis. The sediment samples were disaggregated before grain size analysis using ultrasonification after treatment with hydrogen peroxide and carbonates were removed using calgon. Sand was separated by wet sieving and accounted for 1.8% of the bed sediment. The grain size distribution of fines was measured using a Sedigraph 5100. Silt and clay represent 86.2 and 12.0% of the bed sediment, respectively, which resulted in a mean grain size of 6 φ with standard deviation of 1.6 φ.

The OBS was calibrated in a specially designed calibration

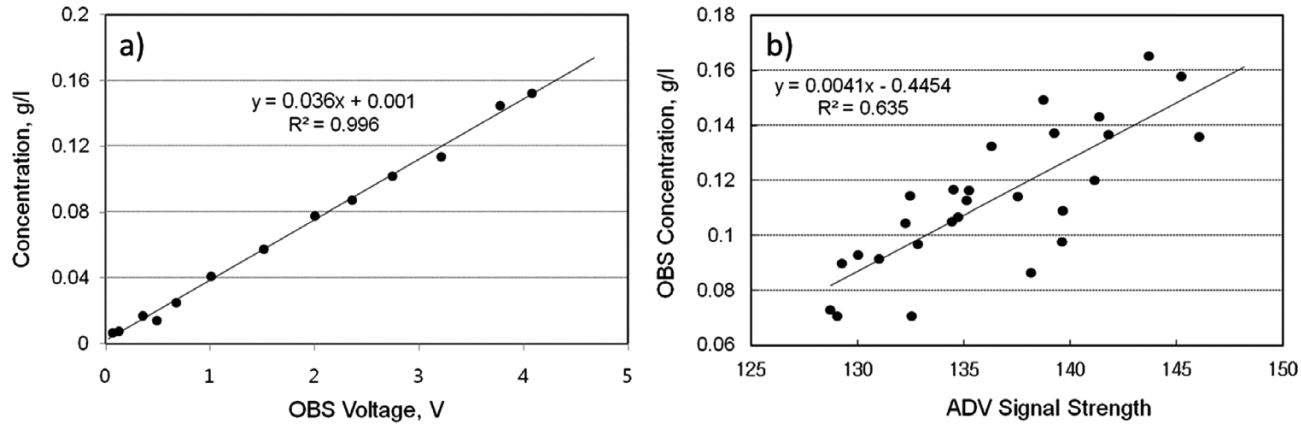


**Fig. 2.** Calibration of OBS and ADV. a) OBS calibration with *in situ* sediment samples in a specialized calibration tank at Inha University; b) Calibration of ADV signal strength against OBS concentration

tank at the Inha University using sediments taken from the bed at the beginning of the experiment. Figure 2a shows the comparison of the OBS voltage measurement and suction samples at the same height of OBS in the calibration tank. The linear regression of concentration against OBS voltage produced a best fit with an $R^2$ value of 0.996. To obtain SSC over the whole period, ADV signal strength was calibrated with the OBS concentration. Despite the lower $R^2$ value (= 0.64), a reasonable fit was produced (Fig. 2b).

## 3. Results

### Variation of current and wave conditions

The field experiment was conducted during a major storm event that coincided with a spring tide (Fig. 3). The spring tidal range, observed at the nearby Incheon tidal station operated by the Korea Hydrographic and Oceanographic Administration, exceeded 9 m with more than 1 m of diurnal inequality. With the onset of the storm, winds blew from the northwest at about 10 m/s. As the front passed the area, the wind direction veered to the northeast with a slight increase in wind speed. The storm generated large waves in the area. The wave height measured at the KMA's Deokjeok wave buoy (37°14'33"N, 126°01'20"E), which is located about 60 km southwest from the study area, recorded wave heights exceeding 2.5 m at the peak of the storm. However, wave height did not exceed more than 1 m at KMA's Incheon station because of wave energy dissipation over the extensive sand ridges in Gyeonggi Bay and also depth-limited wave height on the tidal flat. Although a wave period of 7–8 seconds was observed during the storm at the offshore buoy, short waves with period of 4–5 seconds were typical in the Gyeonggi Bay (Fig. 3).

The field observation covered three days of a spring tide, during which the maximum tidal range was 4.29 m on Day 8 and the minimum range 2.42 m on Day 7 (Fig. 4). Since the study site was located on the upper part of the tidal flat, the averaged time of submergence was reduced to 4 hours and 40 minutes over a tidal cycle with the longest submergence (5 hours and 20 minutes) occurring during the tidal cycle of maximum tidal range. The current speed in the channel varied sinusoidally and decreased to almost zero during the high-tide

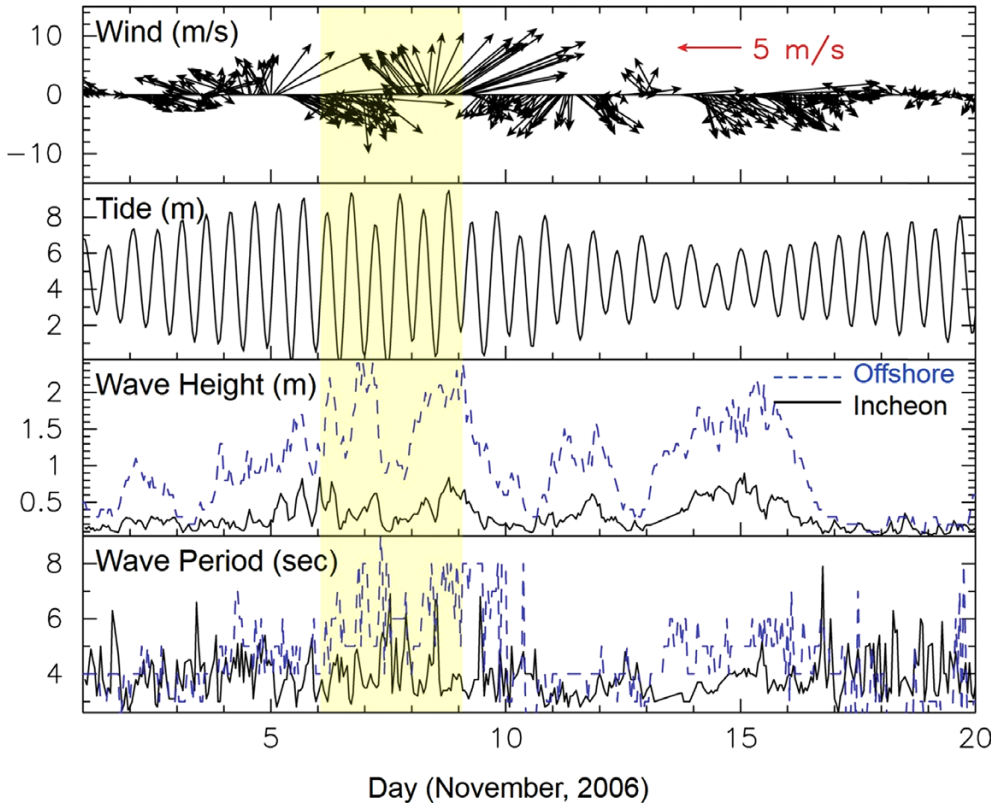


**Fig. 3.** Environmental conditions during November 2006. a) Wind vector observed nearby KMA Incheon Station; b) Tide observed at KHOA Incheon tidal station; c) Wave height observed at Incheon (blue solid) and Deokjeok (black dash); d) wave period observed at Incheon (blue solid) and Deokjeok (black dash). The shaded area indicates the period of field experiment

slack. The current was directed to the north during flood, whereas it was directed to the south during ebb. However, the current direction during ebb was not straight to the south, reflecting the channel geometry. Therefore, the current direction was rotated 12.5 degree clockwise in the preceding data analysis. The maximum current speed (81 cm/s) was observed during the ebb on Day 8 when the maximum tidal range occurred.

Waves were generally small, on the order of 10 cm, with two periods of significant wave activity: one during flood and the other during ebb. During the high slack water, the depth is small enough for the small waves to affect the bottom. The wave heights during the flood and ebb ranged from 10–15 cm, but dropped to about 3 cm during the high-tide slack.

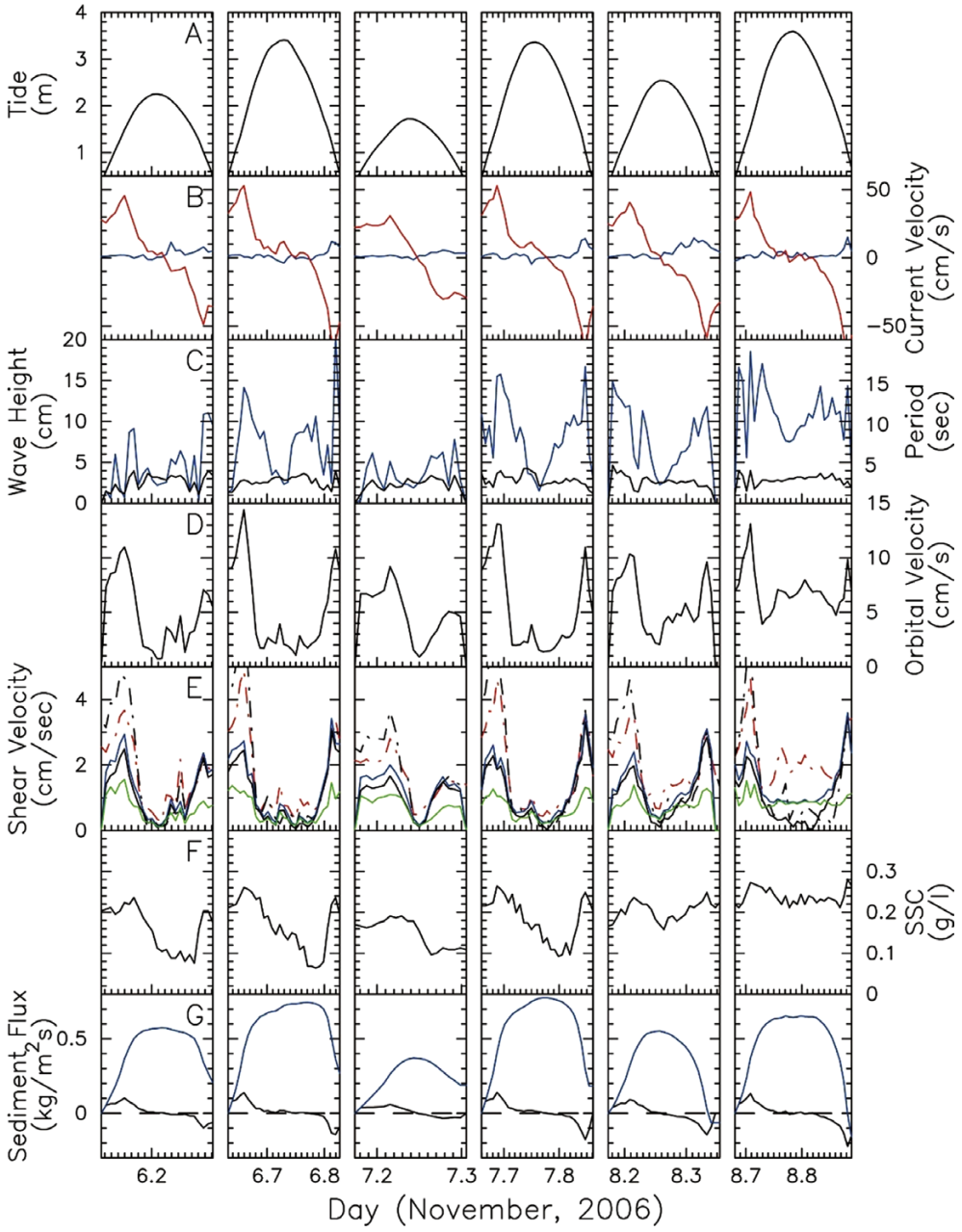


**Fig. 4.** Time-series of A) tide, B) current velocity (red solid – along-channel north-south; blue – cross-channel velocity), C) wave characteristics (blue - wave height; black – wave period), D) wave orbital velocity, E) shear velocity (black dash – $u_{*c\_idm}$; red dash – $u_{*c\_tke}$; black solid – $u_{*c\_gm}$; blue solid – $u_{*cw\_gm}$; green solid – $u_{*w\_gm}$), F) suspended sediment concentration at the nominal elevation of 27 cm ab, and G) sediment flux (black – sediment flux; blue – cumulative sediment flux) over 6 tidal cycles. Note that the time-series displays only the period of submergence

However, the wave height increased on Day 8, which corresponds to the period when winds were aligned with the maximum fetch. Moreover, the wave height remained high, above 5 cm, even during the high slack unlike during the other tidal cycles. Waves exhibited fetch-limited short period of 2–4 seconds.

Bed shear velocity and suspended sediment concentration

The estimated bed shear velocities are shown in Figure 4d. In Figure 4d, the black line indicates the shear velocities, $u_{*c\_idm}$, estimated by the inertial dissipation method of w-velocity component, while the red line indicates the shear velocities, $u_{*c\_tke}$, estimated by the turbulent kinetic energy method. The shear velocities are in phase with the tidal currents, where maximum shear velocities coincide with maximum current velocities of both flood and ebb. However, there exists an inequality of shear during a tidal cycle; the shear is stronger during flood than ebb. The strong shear velocity of 4–5 cm/s decreased almost to zero during the high slack. A relatively strong shear of about 2 cm/s was observed during the high-tide slack on the last tidal cycle. This period corresponds to the wind event with the maximum fetch and is associated with strong wave height (Figs. 3 and 4c).

The shear velocities, modeled using the GM wave-current interaction model, are also shown in Figure 4d. Their behavior is quite similar to the shear velocities estimated from the flow data with peaks corresponding to the acceleration phase of flood and ebb, with a minimum occurring during the high tide slack. During the high-tide slack of the last tidal cycle, however, the shear velocity, due to the combined effects of waves and current, $u_{*cw\_gm}$, did not correspond to $u_{*c\_tke}$, but was equivalent to $u_{*c\_idm}$ and $u_{*c\_gm}$.

Figure 4f shows the time-series of SSC observed by the OBS and ADV. Note that the OBS concentration was saturated at about 0.18 g/l due to high voltage gain. The observed SSC ranged from 0.07 to 0.3 g/l. During the acceleration phase of flood and ebb, SSC was relatively higher in the range of 0.2 g/l, while it dropped to about 0.1 g/l during the high-tide slack for most of the tidal cycles. However, the concentration was maintained at as much as 0.2 g/l during the high-tide slack on September 8.

**Sediment flux**

From a morphological perspective, it is important to assess the effects of waves on the net sediment flux over a tidal cycle. The sediment flux, $Q_s$, was calculated as the product of SSC and velocity at a point, and the cumulative sediment flux was calculated over a tidal cycle from the start of the flood tide to the end of the following ebb tide. The along-channel component of velocity, v, is used in the calculation of sediment flux since the channel is running north-south, and the ebb velocity was rotated 12.5 degrees clockwise.

The sediment flux is directed landward (seaward) during flood (ebb) following the current direction. Moreover, the sediment flux followed the general pattern of two peaks, mid-flood and mid-ebb, with a peak value of about 0.1 kg $m^{-2}s^{-1}$. This is not at all surprising because current velocities and SSCs showed similar behavior. The cumulative sediment flux was usually directed landward during the first four tidal cycles when waves were relatively weak. On the other hand, it was directed seaward during the last two tidal cycles when waves were relatively stronger.

## 4. Discussion

Wind waves and wind-generated shear are important mechanisms responsible for sediment erosion and sediment transport on tidal flats. We had a unique opportunity to capture a strong wave event at the southern Gangwha tidal flats. In this section, we discuss the characteristics of current- and wave-induced turbulence during both calm conditions and wave events.

**Under calm conditions without strong waves**

Under calm conditions without strong waves, the observations resembled the typical behaviors on tidal flats: two peaks of current speed, wave height, bed shear velocity, SSC and sediment flux at mid-tide during both flood and ebb (Christie et al. 1999; Green and Coco 1997, 2014; Le Hir et al. 2000; Talke and Stacey 2008). The maximum flood velocity occurs at mid-tide usually at a height of 1.4–1.6 m above the bed; after a long high-tide slack, the ebb velocity progressively increases toward the end of the tidal phase at the water level of ~1 m. The peak of wave height does not coincide with the peaks of current speed. On the other hand, the peaks of bed shear and SSC correspond to the peak of current speed, suggesting that current is the main forcing under these conditions. This study also indicates that under calm conditions without strong waves the net sediment flux was directed onshore due to the scour and settling lag effects. Sediments were eroded during the flood tide, transported onshore, and settled down during the high-tide slack. Owing to relatively weak currents and shear during the ebb, onshore sediment transport is insignificant.

The net onshore sediment flux at the Gangwha tidal flats matches with the tidal flat processes during calm conditions observed in many tidal flats around the world (Christie et al. 1999; Green and Coco 2014; Le Hir et al. 2000; Talke and Stacey 2008; Zhu et al. 2017)

**Under strong waves**

The East Donggum tidal flat is generally protected from the waves generated in Gyeonggi Bay. Under strong wind conditions, the wave height increases from about 10 cm to about 15–20 cm. Most significant among these wind events was the one on November 8 when waves did not diminish during the high-tide slack. A contour plot of the energy spectra of u- and w-components in Figure 5 demonstrate the wave effects on turbulence. Under calm conditions, spectral density is generally higher during the flooding and ebbing tide, when the current velocity is stronger, than during the high-tide slack (Fig. 5). During the flooding and ebbing tide, the spectra exhibited no wave energy, but current-generated turbulence (Fig. 6a, d) is clearly shown by a -5/3 slope in the inertial subrange. As water depth increases with increasing wave height and slightly decreasing currents, the spectra exhibited small peaks at wave frequencies in the u- and v-components (Fig. 6b). Simultaneously the current-induced spectral energy in the inertial subrange decreased about 2 orders of magnitude compared to the case of Figure 6a. During the high-tide slack, clear peaks at wave frequency in all velocity components appeared (Fig. 6c). However, the spectra are white at the turbulence frequencies.

Under strong waves over the last two tidal cycles, the spectral behavior during the flood and ebb was similar to the behavior under the calm conditions (Fig. 5). However, the

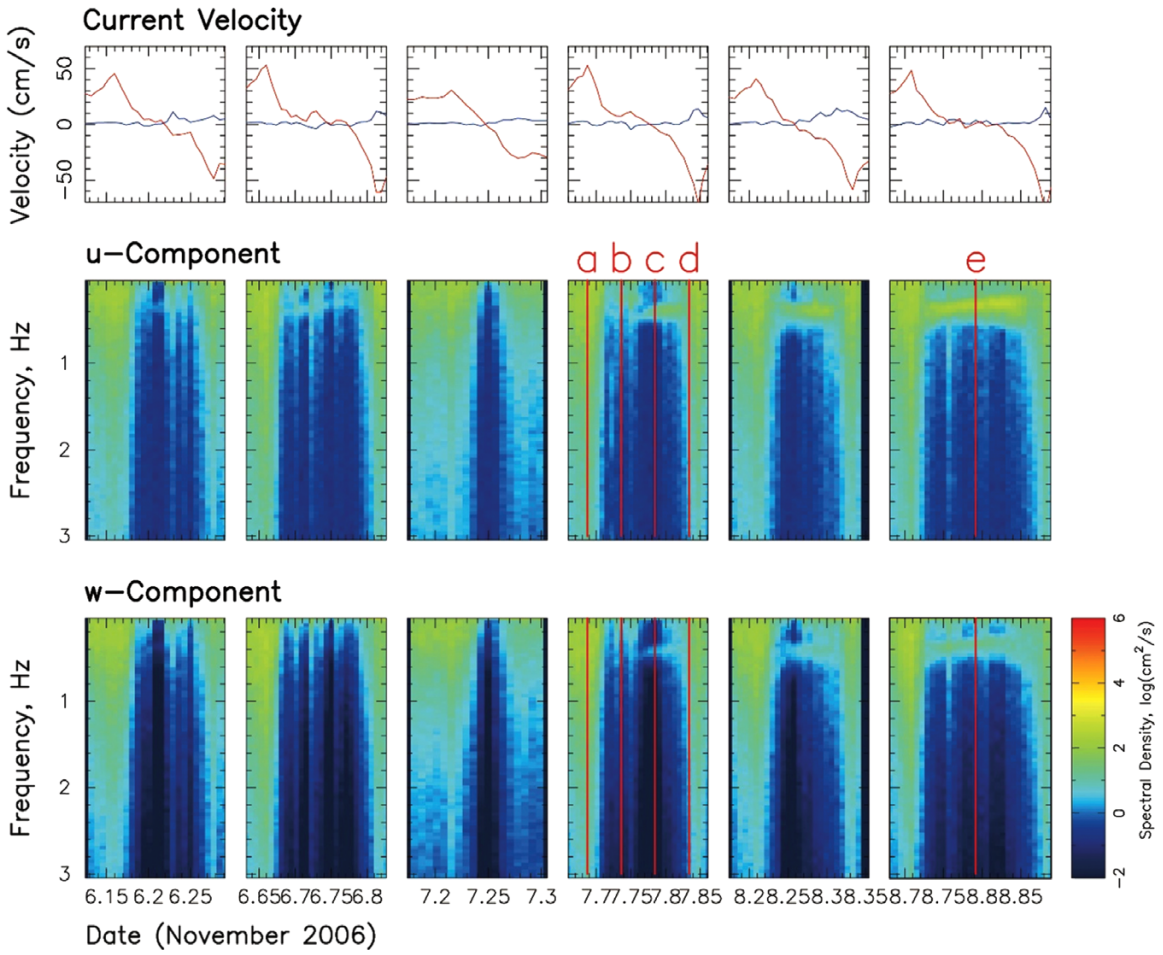


**Fig. 5.** Contour plot of spectral density of u- and w-components of flow velocity, and corresponding current velocities. The turbulence intensity was stronger during the flood and ebb phases, but usually diminished during the high-water slack. However, strong spectral energy was present in the wave frequencies during the high-water slack over the last two tidal cycles. The letters, a-e, indicate the exemplary bursts for which individual spectral densities are shown in Figure 6

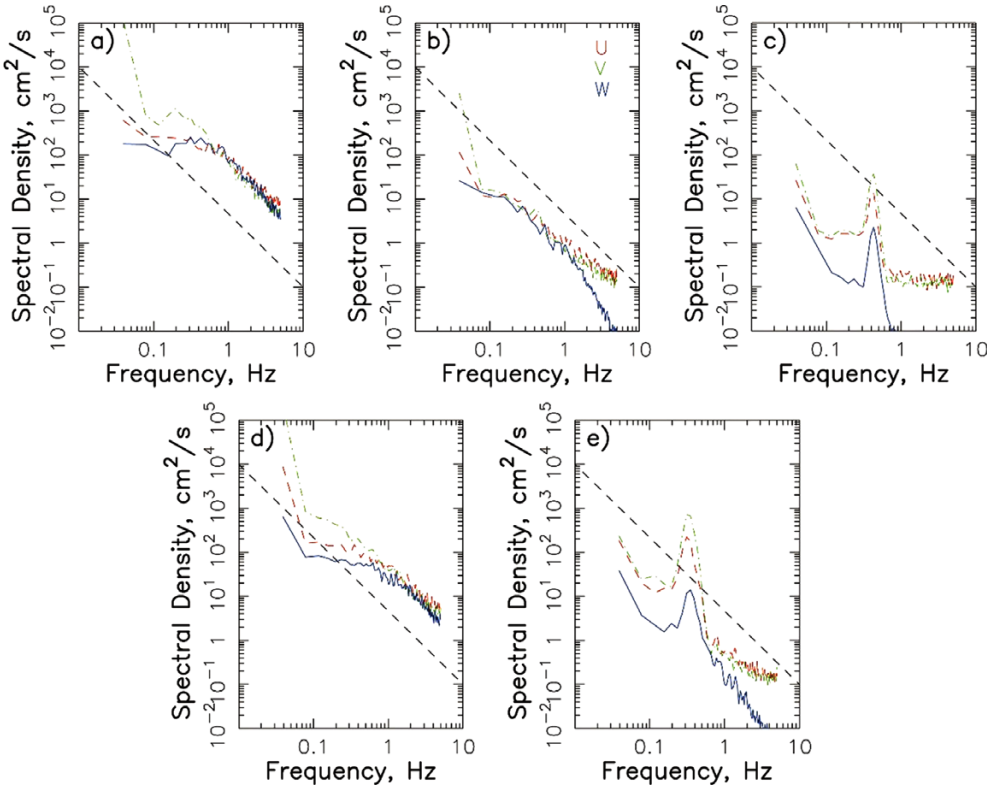


**Fig. 6.** Spectra of horizontal (u and v) and vertical (w) velocities of the five periods (a, b, c, d, and e) shown on Figure 5. Here, a) and d) represent flood and ebb, respectively, while b) and c) represent just before high tide and high tide slack during weak waves. On the other hand, e) represents the spectra of high tide slack under strong waves. A -5/3 slope associated with the inertial subrange is indicated as the dotted line for comparison

spectra density during the high-tide slack was one order of magnitude higher (Fig. 6e) than the spectral density under the calm conditions (Fig. 6c). Moreover, there existed a -5/3 slope on the inertial subrange. Since the current velocity was essentially zero during the high-tide slack (Fig. 5), the turbulence present at this period appears to be induced by waves. Then, this wave-induced turbulence must be responsible for maintaining sediment suspension during the slack period.

The estimated and modeled shear velocities exhibited peaks during the flood and ebb with a minimum during high-tide slack under weak wave conditions. However, the estimated shear velocity by the TKE method, $u_{*c\_tke}$, was much higher during the high-tide slack under strong wave conditions than other periods, while other shear velocities decreased to minima as in other periods. Based on the fact that $u_{*c\_tke}$ includes variance from both waves and turbulence in the estimation of shear velocity, this result indicates that wave variance may have contributed to the enhanced shear during this quiescent period.

Our observation of wave-induced turbulence during the high-tide slack is unique in that waves only generate turbulence to maintain sediment during the high slack. Most previous studies reported that under storm conditions, strong waves dominate or enhance the total shear during the flood phase of tide. The large shear erodes sediment and maintains it in suspension during the high tide slack, inducing net offshore sediment flux (Andersen and Pejrup 2001; Bassoullet et al. 2000; Hunt et al. 2017; Zhu et al. 2017). In addition, Zhu et al. (2016) suggested that during the high-tide slack winds can not only enhance wave shear by increasing wave height, but also increase current shear by superimposing wind-driven turbulent velocities onto the vertical velocities. In these cases, the combined shear erodes sediments in the wave boundary layer and the current shear diffuses them well above the wave boundary layer. However, our observations preclude strong waves during the flood, as well as increased current shear during the high-tide slack. That is, the turbulence existed well above the wave boundary layer, for which the thickness is less than a centimeter. The generation of the wave-induced turbulence above the wave boundary layer is attributable to

the wave-turbulence interaction observed in the upper oceans (Kitaigorodskii and Rumley 1983; Anis and Moum 1995; Ghantous and Babanin 2014). Nonetheless, the mechanism for wave-turbulence interaction in the bottom boundary layer is not well understood and is a topic for further research.

**Ramification to overall sediment transport and morphologic change**

The Gangwha tidal flats underwent rapid changes due to anthropogenic interventions around Gangwha and Yeongjong Islands, in particular the large-scale reclamation of land around Yeongjong Island to construct Incheon International Airport as well as the Gimpo and Songdo land reclamations. Using remote sensing images, Lee et al. (2011) found that deposition has been dominant on the southern Gangwha tidal flat and attributed these changes to the modified tide and current patterns around the tidal flats.

On a tidal flat such as Gangwha, the wind can affect current directions and thus the sediment fluxes. On protected tidal flats where tidal channels are deep and wide, most sediment transport occurs through the tidal channels. The sediment flux through the tidal channel counterbalances the erosion or accretion of the tidal flats. On the East Donggum tidal flat, sediment flux was directed landward under calm conditions, but directed offshore under strong wave conditions (Fig. 4g). To determine the morphologic trend of the tidal flat in response to erosion or accretion based on the direction of sediment flux under wave conditions, we examined the wave height distribution observed at Gangwha tidal flats by the Korea Institute of Ocean Science and Technology from August 1, 2006 through July 31, 2007 (Fig. 7). The wave event observed at the tidal channels of the East Donggum tidal flat is equivalent to a wave height of 0.6 m and wave height greater than 0.6 m account for only 2.2% of total wave height in a year. Therefore, accretion appears to be dominant on the East Donggum tidal flat. In fact, this area was reported as experiencing rapid deposition due to anthropogenic interventions (Lee et al. 2011).

This study indicates that under calm conditions without strong waves the sediment flux was directed onshore due to the scour and settling lag effects, prompting accretion on the upper tidal flat. On the other hand, the sediment flux was directed offshore under strong wave events where wave-induced shear kept sediments in suspension during the high-tide slack and then subsequent ebb currents transported sediments offshore. On the East Donggum tidal flat, the occurrence of strong waves accounts for only about 2.2% of the time of the year. However, other regions which are not as protected from waves as East Donggum may experience more erosion due to the sustained influence of waves that maintains the suspended sediment concentration during the high-tide slack in addition to wave-enhanced erosion during

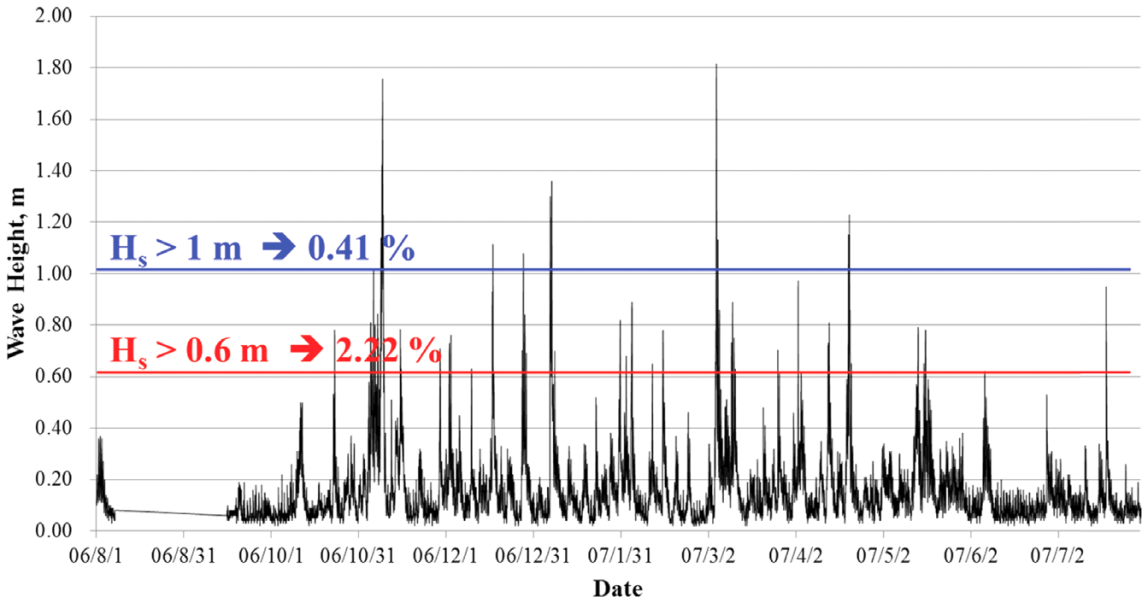


**Fig. 7.** Time-series of wave height observed over a year (August 1, 2006–July 31, 2007) at Gangwha tidal flat by the KIOST wave buoy. The location of the KIOST wave buoy is shown on Figure 1. The equivalent wave height of 1 m, responsible for offshore sediment flux, is shown on the figure

the flood. Therefore, this mechanism of erosion must be considered in examining sediment transport and morphologic changes in other tidal flats of the world.

## 5. Concluding Remarks

Regarding tidal flats, sediment transport is mainly controlled by the tide. Although secondary, waves have been known to enhance bed shear to support higher suspended sediment concentrations than the tide alone. On the East Donggum tidal flat, we had a unique opportunity to observe strong wave-induced shear during high-tide slack when tidal current velocity was essentially zero and thus current-induced shear was no longer present. The wave-induced shear supported sediment suspension during the high-tide slack, which contributed to the offshore flux during the tidal cycle in contrast to the onshore flux due to the conventional scour and settling lag effects. Although the maintenance of sediment suspension caused offshore flux under strong wave events, the occurrence of strong waves on the East Donggum tidal flat rarely takes place. Therefore, this region is experiencing rapid accretion. However, it could be an important mechanism for the offshore flux of sediment and erosion of tidal flats where, under strong waves, wave-induced shear maintenance of a sediment suspension during the high-tide slack is more common. Moreover, the mechanism for wave-induced shear remains poorly documented with the current dataset including a single point measurement from an ADV. Accordingly, this must be a topic of future research.

## Acknowledgements

This research was supported by the Ministry of Oceans and Fisheries of Korea under the research program entitled, 'Development of Integrated Estuarine Management System', and by Inha University Research Grant. We would like to thank Kyungsik Choi and two anonymous reviewers for their constructive comments on the earlier version of this manuscript.

## References

Andersen TJ, Pejrup M (2001) Suspended sediment transport on a temperate, microtidal mudflat, the Danish Wadden Sea. Mar Geol **173**:69–85

Anis A, Moum JN (1995) Surface wave-turbulence interactions: scaling e(z) near the sea surface. J Phys Oceanogr **25**:2025–2045

Bassoullet P, Le Hir P, Gouleau D, Robert S (2000) Sediment transport over an intertidal mudflat: field investigations and estimation of fluxes within the "Baie de Marennes-Oleron" (France). Cont Shelf Res **20**:1635–1653

Brand A, Lacy JR, Hsu K, Hoover D, Gladding S, Stacey MT (2010) Wind-enhanced resuspension in the shallow waters of South San Francisco Bay: mechanisms and potential implications for cohesive sediment transport. J Geophys Res **115**:C11024. doi:10.1029/2010JC006172

Bendat JS, Piersol AG (2010) Random data: analysis and measurement procedures (4th ed). Wiley, New York, 640 p

Bricker JD, Monismith SG (2007) Spectral wave-turbulence decomposition. J Atmos Ocean Tech **24**:1479–1487

Carlin JA, Lee G, Dellapenna TM, Laverty P (2016) Sediment resuspension by wind, waves, and currents during meteorological frontal passages in a micro-tidal lagoon. Estuar Coast Shelf S **172**:24–33

Choi KS, Dalrymple RW (2004) Recurring tide-dominated sedimentation in Kyonggi Bay (west coast of Korea): similarity of tidal deposits in late Pleistocene and Holocene sequences. Mar Geol **212**(1–4):81–96

Choi JK, Eom J, Rye JH (2011) Spatial relationships between surface sedimentary facies distribution and topography using remotely sensed data: example from the Gangwha tidal flat, Korea. Mar Geol **280**:205–211

Chrisitie MC, Dyer KR, Turner P (1999) Sediment flux and bed level measurements from a macro tidal mudflat. Estuar Coast Shelf S **49**:667–688

Ghantous M, Babanin AV (2014) One-dimensional modeling of upper ocean mixing by turbulence due to wave orbital motion. Nonlinear Proc Geoph **21**:325–338

Grant WD, Madsen OS (1986) The continental shelf bottom boundary layer. Annu Rev Fluid Mech **18**:265–305

Green MO, Coco G (2007) Sediment transport on an estuarine intertidal flat: measurements and conceptual model of waves, rainfall and exchanges with a tidal creek. Estuar Coast Shelf S **72**:553–569

Green MO, Coco G (2014) Review of wave-driven sediment resuspension and transport in estuaries. Rev Geophy **52**:77–117

Hu, Z, Yao P, van der Wal D, Bouma TJ (2017) Patterns and drivers of daily bed-level dynamics on two tidal flats with contrasting wave exposure. Sci Rep **7**:7088

Hunt S, Bryan KR, Mullarney JC (2017) The effect of wind waves on spring-neap variations in sediment transport in two meso-tidal estuarine basins with contrasting fetch. Geomorphology **280**:76–88

Janssen-Stelder B (2000) The effect of different hydrodynamic conditions on the morphodyanics of a tidal mudflat in the

Dutch Wadden Sea. Cont Shelf Res **20**:1461–1478

Kim SC, Friedrichs CT, Maa JPY, Wright LD (2000) Estimating bottom stress in tidal boundary layer from acoustic Doppler velocimeter data. J Hydraul Eng-ASCE **126**:399–406

Kitaigorodskii SA, Lumley JL (1983) Wave-turbulence interactions in the upper ocean. Part I: the energy balance of the interacting fields of surface wind waves and wind-induced three-dimensional turbulence. J Phys Oceanogr **13**:1977–1987

Le Hir P, Roberts W, Cazaillet O, Christie M, Bassoullet P, Bacher C (2000) Characterization of intertidal flat hydrodynamics. Cont Shelf Res **20**:1433–1459

Lee G, Friedrichs CT, Vincent CE (2002) Examination of diffusion versus advection dominated sediment suspension on the inner shelf under storm and swell conditions, Duck, North Carolina. J Geophys Res **107**(C7):21-1–21-22

Lee G, Dade BD, Friedrichs CT, Vincent CE (2003) Spectral estimates of bed shear stress using suspended-sediment concentrations in a wave-current boundary layer. J Geophys Res **108**(C7):3208

Lee YK, Ryu JH, Choi JK, Soh JG, Eom JA, Won JS (2011) A study of decadal sedimentation trend changes by waterline comparisons within the Gangwha tidal flats initiated by human activities. J Coastal Res **27**(5):857–869

MacVean LJ, Lacy JR (2014) Interactions between waves, sediment, and turbulence on a shallow estuarine mudflat. J Geophy Res **119**:1534–1553

Shaw WJ, Trowbridge JH (2001) The direct estimation of near-bottom turbulent fluxes in the presence of energetic wave motions. J Atmos Ocean Tech **18**:1540–1557

Shi B, Wang YP, Du X, Cooper JR, Li P, Li ML, Yang Y (2016) Field and theoretical investigation of sediment mass fluxes on an accretional coastal mudflat. J Hydro-Environ Res **11**:75–90

Soulsby RL, Dyer KR (1981) The form of the near-bed velocity profile in a tidally accelerating flow. J Geophys Res **86**:8067–8074

Soulsby R (1983) The bottom boundary layer of shelf seas. In: Johns B (ed) Physical oceanography of coastal and shelf seas, vol. 35. Elsevier, Amsterdam, pp 189–266

Talke SA, Stacey MT (2008) Suspended sediment fluxes at an intertidal flat: the shifting influence of wave, wind, tidal, and freshwater forcing. Cont Shelf Res **28**:710–725

Thornton EB (1979) Energetics of breaking waves within the surf zone. J Geophys Res **84**:4931–4938

Tucker MJ, Pitt EG (2001) Waves in ocean engineering, vol. 5. Elsevier, Amsterdam, 548 p

Verney R, Deloffre J, Brun-Cottan JC, Lafite R (2007) The effect of wave-induced turbulence on intertidal mudflats: impact of boat traffic and wind. Cont Shelf Res **27**:594–612

Woo HJ, Je JG (2002) Changes of sedimentary environments in the southern tidal flat of Gangwha island. Ocean Polar Res **20**(2):331–343 (in Korean)

Xu JP, Wright LD (1995) Tests of bed roughness models using field data from the Middle Atlantic Bight. Cont Shelf Res **15**:1409–1434

Zhu Q, van Prooijen BC, Wang ZB, Ma YX, Yang SL (2016) Bed shear stress estimation on an open intertidal flat using in site measurements. Estuar Coast Shelf S **182**:190–201

Zhu Q, van Prooijen BC, Wang ZB, Yang SL (2017) Bed-level changes on intertidal wetland in response to waves and tides: A case study from the Yangtze River Delta. Mar Geol **385**: 160–172